SCIENTIFIC REPORTS

OPEN

SUBJECT AREAS:
CHEMISTRY
BIOCHEMISTRY

Received
4 November 2013

Accepted
24 January 2014

Published
25 February 2014

Correspondence and requests for materials should be addressed to Y.L. (yuliu@nankai.edu.cn)

# Polysaccharide-Gold Nanocluster Supramolecular Conjugates as a Versatile Platform for the Targeted Delivery of Anticancer Drugs

Nan Li[1], Yong Chen[1], Ying-Ming Zhang[1], Yang Yang[1], Yue Su[1], Jia-Tong Chen[2] & Yu Liu[1]

[1]Department of Chemistry, State Key Laboratory of Elemento-Organic Chemistry, Collaborative Innovation Center of Chemical Science and Engineering (Tianjin), Nankai University, [2]Department of Biochemistry and Molecular Biology, College of Life Sciences, Nankai University, Tianjin 300071, P.R. China.

**Through the high affinity of the *β*-cyclodextrin (*β*-CD) cavity for adamantane moieties, novel polysaccharide-gold nanocluster supramolecular conjugates (HACD-AuNPs) were successfully constructed from gold nanoparticles (AuNPs) bearing adamantane moieties and cyclodextrin-grafted hyaluronic acid (HACD). Due to their porous structure, the supramolecular conjugates could serve as a versatile and biocompatible platform for the loading and delivery of various anticancer drugs, such as doxorubicin hydrochloride (DOX), paclitaxel (PTX), camptothecin (CPT), irinotecan hydrochloride (CPT-11), and topotecan hydrochloride (TPT), by taking advantage of the controlled association/dissociation of drug molecules from the cavities formed by the HACD skeletons and AuNPs cores as well as by harnessing the efficient targeting of cancer cells by hyaluronic acid. Significantly, the release of anticancer drugs from the drug@HACD-AuNPs system was pH-responsive, with more efficient release occurring under a mildly acidic environment, such as that in a cancer cell. Taking the anticancer drug DOX as an example, cell viability experiments revealed that the DOX@HACD-AuNPs system exhibited similar tumor cell inhibition abilities but lower toxicity than free DOX due to the hyaluronic acid reporter-mediated endocytosis. Therefore, the HACD-AuNPs supramolecular conjugates may possess great potential for the targeted delivery of anticancer drugs.**

Currently, nanomaterials have attracted significant interest due to their potential applications in drug delivery, sensing, imaging and chemotherapy. Nanomaterials offer advantages in these applications because of their unique physical and chemical properties[1–3]. Among the broad variety of known nanoparticles, gold nanoparticles have been widely studied in various fields, particularly in drug delivery[4,5]. Gold nanoparticles have a number of desirable advantages, including (1) good biocompatibility[6,7], (2) convenient synthesis and facile size control[8], (3) robust stability under most *in vivo* conditions[9], and (4) tunable surface features and dense loading functionalities for specific cell targeting[10,11]. Thus, gold nanoparticles have been used as delivery scaffolds to load various bioactive molecules for cancer therapeutics. To date, numerous effective anticancer drugs have been used for the treatment of various human and animal cancers, such as doxorubicin hydrochloride (DOX), paclitaxel (PTX), camptothecin (CPT), irinotecan hydrochloride (CPT-11), and topotecan hydrochloride (TPT). However, their lack of tumor-targeting ability, poor biodistribution, undesirable side-effects, and low aqueous solubility (in the case of PTX and CPT) have limited their clinical use and development[12–14]. In addition to employing carriers to improve drug solubility, these drawbacks have been overcome by introducing targeting agents that recognize cancer cells. Hyaluronic acid (HA) is an optimal targeting ligand that has been extensively used in targeted drug delivery and cancer therapeutics due to its specific binding affinity for CD44 and RHAMM (the HA receptor over-expressed on cancer cells) as well as its long-acting delivery of biopharmaceuticals[15–18]. In addition, the integration of gold nanoparticles and HA for the loading, delivery and release of drugs as well as the recognition of tumor cells provides numerous advantages. For instance, Sreenivasan and Manju[19] formulated multifunctional gold nanoparticles modified with a hyaluronic acid-curcumin conjugate and a folic acid-polyethylene glycol conjugate that displayed enhanced targeting and improved efficacy compared to free curcumin. Park and co-workers[20] developed gold nanoparticles functionalized with

near-infrared fluorescence dye-labeled HA and investigated their anticancer abilities *in vitro* and *in vivo*, demonstrating that the gold nanoparticles modified with HA could effectively identify metastatic tumors as well as diagnose and treat HA degrading diseases. However, it is noteworthy that, in the majority of studies, drug delivery systems have been utilized with only a single anticancer drug[21–23]. Therefore, considerable effort should be directed toward devising and developing novel platforms for the loading and delivery of a variety of anticancer drugs. In the present work, we designed a drug delivery system, drug@HACD-AuNPs (Fig. 1, see Supporting Information for synthesis details), containing three components: HACD (cyclodextrin-modified hyaluronic acid), AuNPs (gold nanoparticles bearing adamantane moieties), and an anticancer drug (DOX, PTX, CPT, CPT-11, and TPT, structures shown in Fig. 2). In this supramolecular conjugate, the porous nanocluster HACD-AuNPs could be stably constructed due to the strong affinity between the $\beta$-CD cavity and adamantane moieties[24]. Various types of anticancer drugs could be efficiently loaded into the three-dimensional porous structure using hydrophobic and electrostatic interactions, resulting in drug@HACD-AuNPs that were beneficial in targeted drug delivery and controlled release applications. Although cyclodextrin cavities are also able to carry anticancer drugs, their inclusion abilities are rather limited. For example, the complex stability constants for $\beta$-CD with DOX[25], PTX[26], and CPT[27] are reported to be 188 $M^{-1}$, 300 $M^{-1}$, and 266 $M^{-1}$, corresponding to approximate encapsulation efficiencies of 7.5%, 21.0%, and 15.8%, respectively. When loading various anticancer drugs into the porous structure of the HACD-AuNPs nanoclusters through hydrophobic and electrostatic interactions, significantly improved encapsulation efficiencies of 79%, 53% and 47% were observed for DOX, PTX, and CPT, respectively.

## Results and Discussion

**Characterization of adamantylamine-modified gold nanoparticles (AuNPs).** Adamantylamine-modified gold nanoparticles (AuNPs) were characterized by UV-vis spectroscopy, X-ray photoelectron spectroscopy (XPS), high-resolution transmission electron microscopy (HR-TEM), atomic force microscopy (AFM), elemental analysis, and inductively coupled plasma (ICP). The UV-vis spectrum of the AuNPs showed a weak absorption peak at 514 nm (Supplementary Fig. S4) assigned to the surface plasmon resonance (SPR) band of the AuNPs[28], most likely indicating the formation of small gold nanoparticles[29]. The XPS survey spectrum of the AuNPs (Supplementary Fig. S5) displayed Au4f, Au4d5 and Au4d3 peaks at 84 eV, 334 eV and 353 eV, respectively[30,31]. In addition, TEM images of the AuNPs (Supplementary Fig. S6a) showed a number of well-dispersed spherical particles with an average diameter of 2.2 nm. Similar results were observed in AFM images (Supplementary Fig. S6b), in which the AuNPs were also present as discrete particles. By analyzing the elemental analysis data and ICP data, we concluded that the average number of 1,2-dithiolane-3-pentanamide (amantadine-lipoic acid) units around each nanoparticle was 19, and the average surface area occupied by

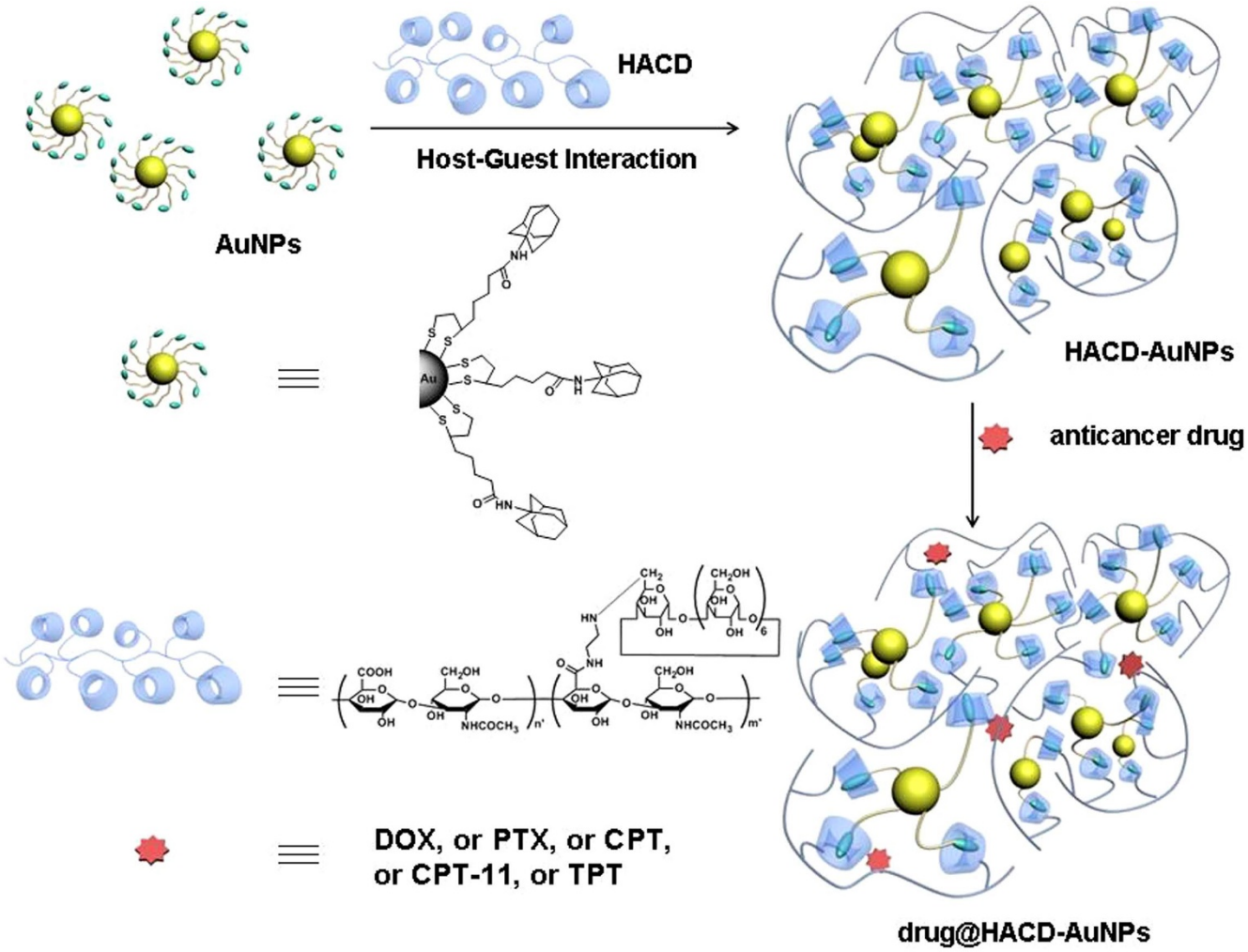


**Figure 1 | Schematic illustration of the chemical structures and construction of the HACD-AuNPs and the drug@HACD-AuNPs.**

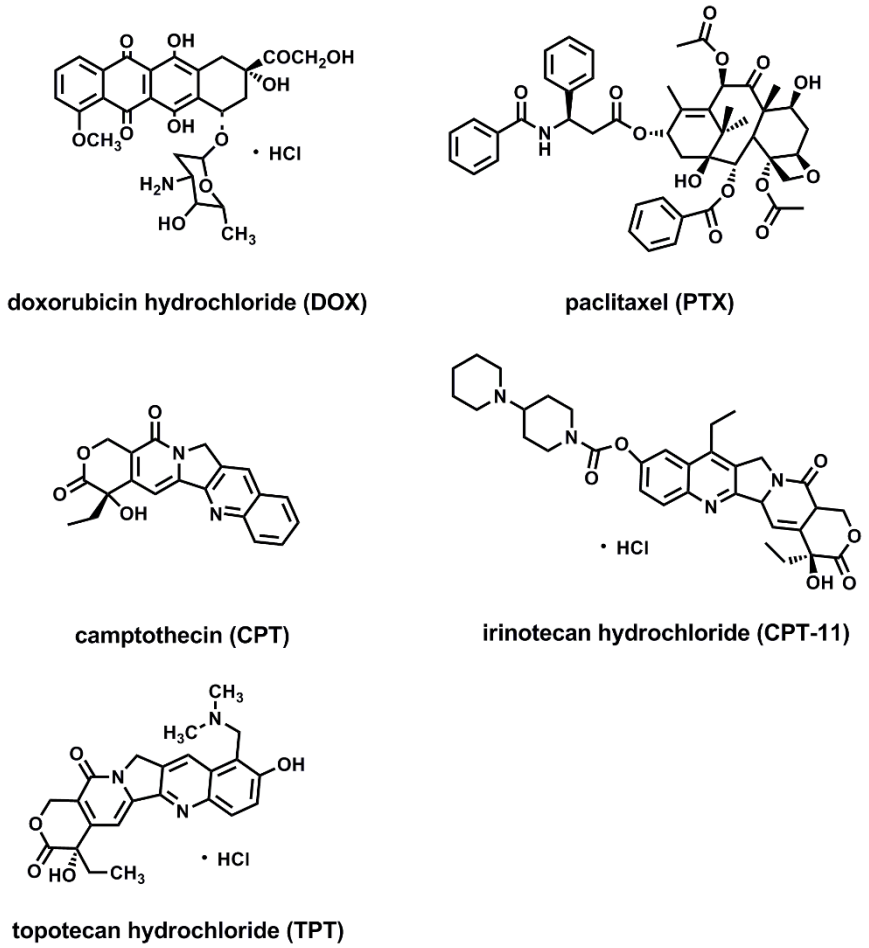


**Figure 2** | **Structures of the anticancer drugs.**

one 1,2-dithiolane-3-pentanamide (amantadine-lipoicacid) unit was 3.20 nm[232].

**Characterization of HACD-AuNPs.** Due to the high affinity of the $\beta$-CD cavity to adamantane moieties, stable supramolecular nanocluster HACD-AuNPs were successfully constructed from gold nanoparticles and HACD. Due to the presence of numerous hydroxyl groups in HACD, the HACD-AuNPs clusters displayed satisfactory water solubility, as indicated by centrifugation experiments at relatively high nanocluster concentrations (Supplementary Fig. S17). Moreover, the greatly strengthened Tyndall effect indicated the formation of large nanoclusters (Supplementary Fig. S18). As observed from the UV-vis spectrum of the HACD-AuNPs (Supplementary Fig. S7), the surface plasmon resonance (SPR) band of the gold particles displayed a bathochromic shift of 26 nm, most likely indicating that the gold nanoparticles aggregated into larger clusters or that the thickness of the adsorbed molecules increased[33,34]. In addition, the originally discrete particles in the AuNPs aggregated to form large clusters in the HACD-AuNPs, as observed in both TEM and AFM images (Fig. 3a and Fig. 3b). Dynamic light scattering (DLS) experiments also confirmed this aggregation, revealing the presence of large nanoclusters of HACD-AuNPs with an average diameter of approximately 258 nm and a narrow size distribution (Fig. 3d). In addition, the zeta potential of the HACD-AuNPs was measured to be approximately −30.99 mV (Supplementary Fig. S15), indicating that the surfaces of the nanoclusters were negatively charged. However, it is important to note that the CDs were reported to barely include the guest molecule in ethanol, and the exclusion of the adamantane moiety of the AuNPs from the CD cavities of HACD will therefore occur in ethanolic solutions. TEM images also demonstrated that, with the addition of ethanol, the HACD-AuNPs disassembled to small discrete particles similar to those observed in the free AuNPs. These results demonstrate that the association of HACD with the AuNPs was driven by weak, non-covalent interactions.

**Drug Loading.** After successfully constructing the HACD-AuNPs nanoclusters, we investigated their loading ability towards various anticancer drugs, such as DOX, PTX, CPT, CPT-11, and TPT. In a typical example, the cationic anticancer drug DOX was selected as a drug model. By measuring the characteristic absorption of DOX at 490 nm, the photometric standard curve of DOX was obtained with absorption intensity as the ordinate and the DOX concentration in milli-Q water as the abscissa (Supplementary Fig. S8). Accordingly, the DOX encapsulation and loading efficiency were calculated to be 78.68% and 11.03%, respectively.

It is well-known that AuNPs act as good quenchers of fluorescence donors due to the nanometal surface energy transfer (NSET) effect[35–37]. As illustrated in Supplementary Fig. S10, the fluorescence intensity of DOX after loading in the HACD-AuNPs decreased by 72%. In addition, the zeta potential of the DOX@HACD-AuNPs was measured to be approximately −18.48 mV, much higher than that of the HACD-AuNPs alone (−30.99 mV, Supplementary Fig. S16), which was ascribed to the loading of the positively charged DOX. It is also noteworthy that, even after the loading of DOX, the nanocluster HACD-AuNPs maintained a negative surface charge, which would diminish the toxicity of the gold nanoparticles[9,38]. These results jointly indicate that the anticancer drug DOX was efficiently loaded onto the HACD-AuNPs to form biocompatible DOX@HACD-AuNPs conjugates. Furthermore, the encapsulation

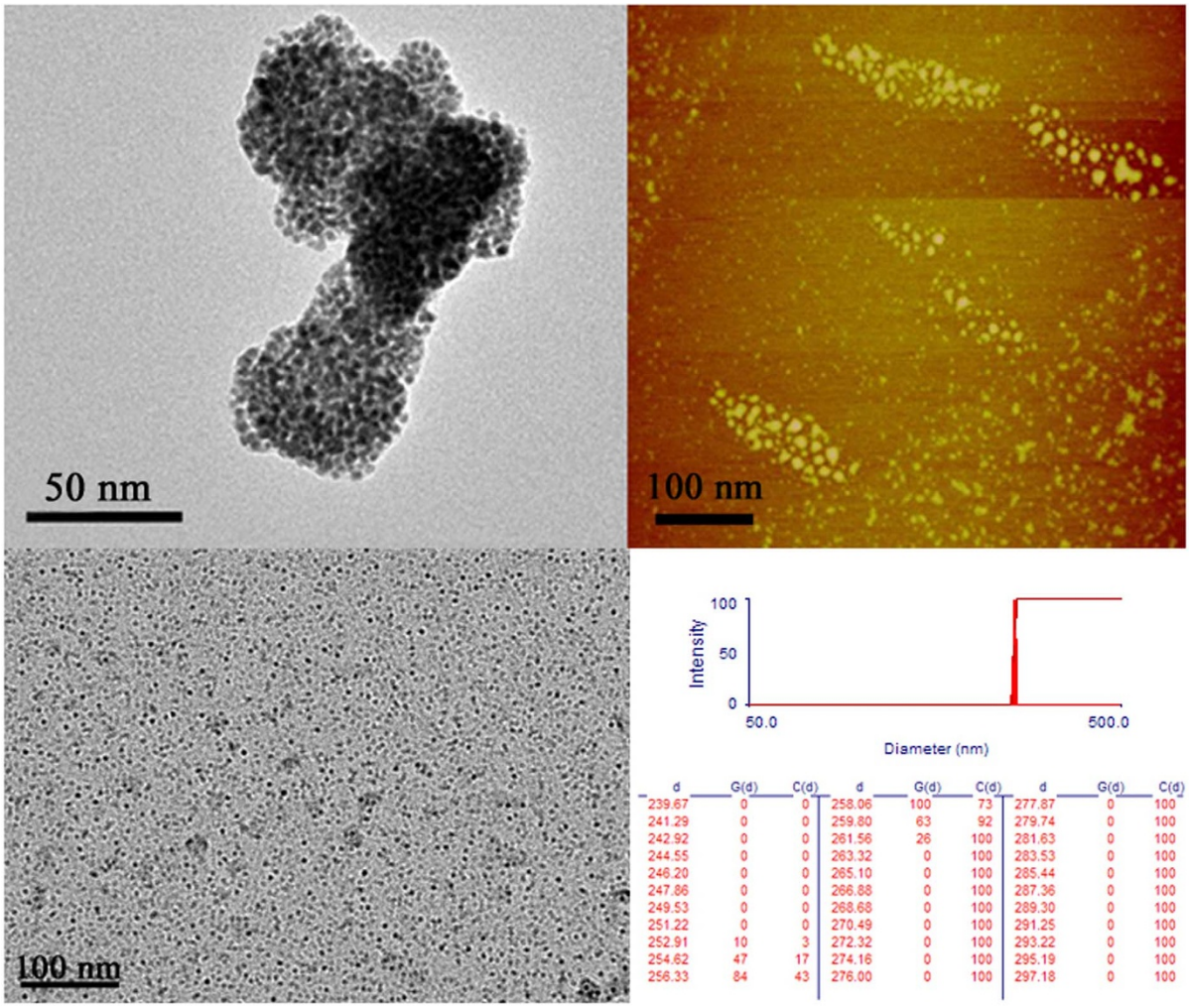


| d | G(d) | C(d) | d | G(d) | C(d) | d | G(d) | C(d) |
|---|---|---|---|---|---|---|---|---|
| 239.67 | 0 | 0 | 258.06 | 100 | 73 | 277.87 | 0 | 100 |
| 241.29 | 0 | 0 | 259.80 | 63 | 92 | 279.74 | 0 | 100 |
| 242.92 | 0 | 0 | 261.56 | 26 | 100 | 281.63 | 0 | 100 |
| 244.55 | 0 | 0 | 263.32 | 0 | 100 | 283.53 | 0 | 100 |
| 246.20 | 0 | 0 | 265.10 | 0 | 100 | 285.44 | 0 | 100 |
| 247.86 | 0 | 0 | 266.88 | 0 | 100 | 287.36 | 0 | 100 |
| 249.53 | 0 | 0 | 268.68 | 0 | 100 | 289.30 | 0 | 100 |
| 251.22 | 0 | 0 | 270.49 | 0 | 100 | 291.25 | 0 | 100 |
| 252.91 | 10 | 3 | 272.32 | 0 | 100 | 293.22 | 0 | 100 |
| 254.62 | 47 | 17 | 274.16 | 0 | 100 | 295.19 | 0 | 100 |
| 256.33 | 84 | 43 | 276.00 | 0 | 100 | 297.18 | 0 | 100 |

**Figure 3** | (a) HR-TEM image of the HACD-AuNPs (scale bar = 50 nm), (b) AFM image of the HACD-AuNPs (scale bar = 100 nm), (c) TEM image of the HACD-AuNPs in the presence of ethanol (scale bar = 100 nm), and (d) DLS results from the HACD-AuNPs.

and loading efficiencies of other selected anticancer drugs were measured and listed in Table 1. From Table 1, it is apparent that the HACD-AuNPs presented satisfactory loading abilities for both hydrophobic and hydrophilic drugs, clearly demonstrating their potential as a versatile platform for the delivery of anticancer drugs.

**Drug release.** The release behavior of the drug@HACD-AuNPs was also investigated to verify their ability as drug carriers to perform controlled release in physiological environments. The drug release profiles of the drug@HACD-AuNPs and the corresponding free anticancer drugs in phosphate buffer solutions ($I$ = 0.01 M) at 37°C are presented in Fig. 4 and Supplementary Figs. S24–S27, wherein different pH values (pH = 5.7 and 7.2) were selected for drug release because they are close to the physiological and endosomal pH values of a cancer cell, respectively. As observed in Fig. 4, the DOX@HACD-AuNPs displayed the slow and controlled release of the drug, with the release rate measured to be 3 or 4 times lower than that of free DOX in acidic or neutral environments, respectively. In addition, the release efficiency of the drug from the DOX@HACD-AuNPs was 3–4 times higher at pH 5.7 (the endosomal pH of a cancer cell) than at pH 7.2 (physiological pH). A similar phenomenon was also observed in the case of PTX (Supplementary Fig. S24). This pH-responsive, preferred release of the drug in cancer cell environments will not only improve its cytotoxic efficacy against tumor cells but also reduce the toxicity of the drug to normal tissues[39]. In addition, it is clear that CPT and its analogues, CPT-11 and TPT, exist in two distinguishable forms (the lactone form and the carboxylate form) under different pH conditions. For this reason, only one pH value (pH = 5.7) was selected for the release of these drugs. From Supplementary Fig. S25 to S27, the CPT@HACD-AuNPs, CPT-11@HACD-AuNPs, and TPT@HACD-AuNPs all displayed the slow and controlled release of their drug, similar to the results with DOX and PTX. Additionally, free CPT showed no appreciable release under the same conditions due to its poor water solubility.

Table 1 | Encapsulation efficiency and loading efficiency of DOX, PTX, CPT, CPT-11, and TPT on HACD-AuNPs. Data were the average of three experiments ± SD

| | DOX | PTX | CPT | CPT-11 | TPT |
|---|---|---|---|---|---|
| Encapsulation efficiency (%) | 78.68 ± 2.52 | 53.17 ± 5.63 | 47.07 ± 5.08 | 45.16 ± 4.51 | 34.65 ± 3.31 |
| Loading efficiency (%) | 11.03 ± 0.31 | 19.47 ± 2.06 | 4.50 ± 0.49 | 7.35 ± 0.74 | 5.04 ± 0.87 |

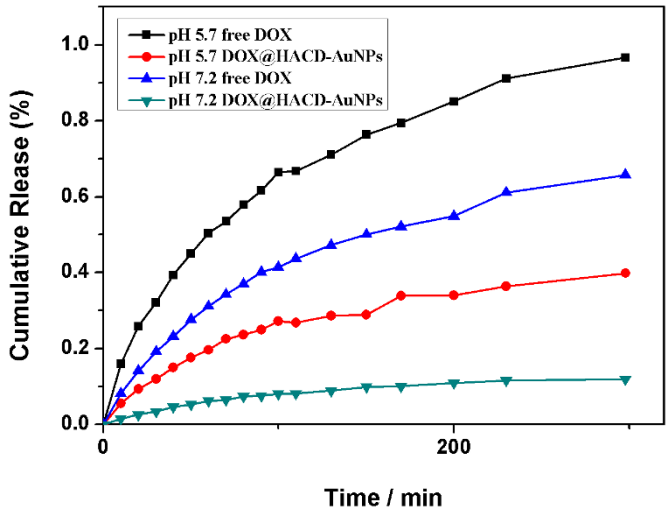


Figure 4 | *In vitro* release profiles of DOX from the DOX@HACD-AuNPs and free DOX in phosphate buffer solution (pH = 5.7 and 7.2, $I$ = 0.01 M) at 37°C.

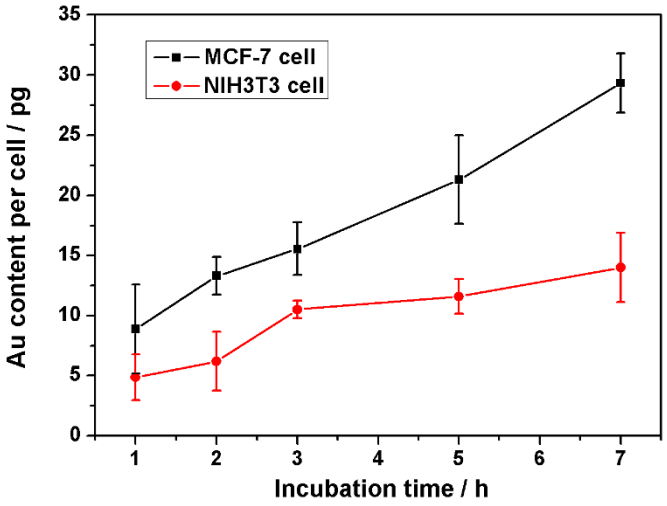


Figure 5 | The cellular uptake of the HACD-AuNPs by MCF-7 and NIH3T3 cells was measured by the Au content per cell. Data were the average of three experiments ± SD.

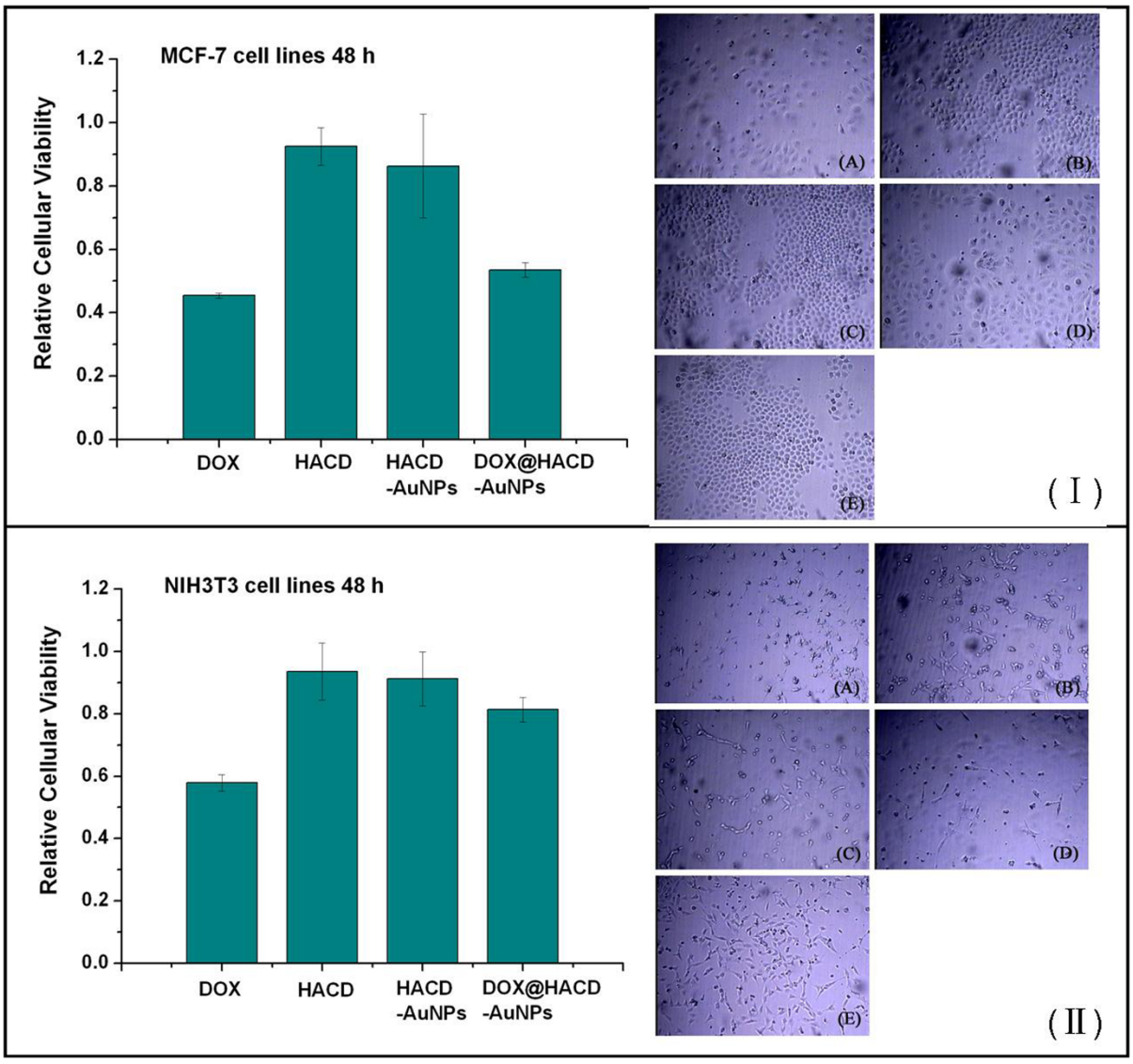


**Figure 6 | Cytotoxicity experiments *in vitro* in 48 h.** The relative cellular viability of MCF-7 cell lines (I left) and NIH3T3 cell lines (II left) 48 h after treatment with DOX, HACD, HACD-AuNPs, and DOX@HACD-AuNPs. Photos of MCF-7 cell lines (I right) and NIH3T3 cell lines (II right) treated with (A) DOX, (B) HACD, (C) HACD-AuNPs, (D) DOX@HACD-AuNPs, and (E) blank are shown.

**Intracelluar uptake.** Human breast cancer MCF-7 cells that abundantly over-express HA receptors (CD44 and RHAMM) on their surfaces[15–18,40] and mouse embryo fibroblast NIH3T3 cells that are HA receptor-negative[41,42] were selected to evaluate the cancer cell targeting and anticancer activity of the DOX@HACD-AuNPs. An analysis of the gold content in the cells was used to evaluate the cellular uptake of the polysaccharide-gold nanoparticle conjugates. Fig. 5 shows the time-dependent gold content of the HACD-AuNPs in MCF-7 and NIH3T3 cells measured by ICP-MS. In the initial 7 h, the cellular gold content increased in an approximately linear manner in MCF-7. At each time interval, the cellular gold content in the MCF-7 cells was higher than that in the NIH3T3 cells. This higher intracellular uptake of the HACD-AuNPs in the MCF-7 cells may have resulted from the association of the HA units in the HACD-AuNPs with the HA receptors on the MCF-7 cell surfaces.

The *in vitro* cytotoxicity of various formulations, including free DOX, HACD, HACD-AuNPs, DOX@HACD-AuNPs, and blank culture media are shown in Fig. 6 and Supplementary Fig. S28. As shown in Fig. 6, the DOX@HACD-AuNPs displayed similar anticancer activity (relative cellular viability 53% *vs* 46%) as free DOX after a 48 h incubation. This result may be due to the specific associations between the HA units on the DOX@HACD-AuNPs and the HA receptors on the cell surfaces, which could facilitate the incorporation and uptake of the DOX@HACD-AuNPs into the MCF-7 cancer cells through receptor-mediated endocytosis, resulting in the release of DOX. Furthermore, the half maximal inhibitory concentration (IC50) of the DOX@HACD-AuNPs was determined by an MTT assay (Supplementary Fig. S29), and the result showed that the DOX@HACD-AuNPs possessed a similar IC50 (IC50 = 60.5 μg $mL^{-1}$) towards the MCF-7 cells as free DOX (IC50 = 43.7 μg $mL^{-1}$)[43] after incubation for 24 h. On the other hand, HACD-AuNPs@DOX gave obviously higher cellular viability (82%) towards the NIH3T3 cells than DOX (57%) after 48 h, indicating the low toxicity of the DOX@HACD-AuNPs. In the control experiments, HACD and the HACD-AuNPs displayed low cytotoxicity toward both the MCF-7 and NIH3T3 cells. In addition, the morphologies of cancer cells and normal cells in the presence of free DOX, HACD-AuNPs, and DOX@HACD-AuNPs (Fig. 6a–6c) also showed that the DOX@HACD-AuNPs exerted a deleterious effect on the cancer cells, similar to free DOX.

## Conclusion

In summary, we developed a new drug delivery system by loading various anticancer drugs onto HACD-AuNPs *via* the three-dimensional, porous structure of the nanoparticle conjugates. Due to the high efficiency of their cellular uptake by HA reporter-mediated endocytosis, the resulting drug@HACD-AuNPs effectively inhibited the growth of MCF-7 cells, enabled pH-responsive drug release in cells, and decreased the drug toxicity toward normal cells. Consequently, these results suggested that this nanocluster will facilitate therapeutic efficacy. Furthermore, this nanocluster, as a useful carrier, could provide new possibilities in the development of targeted drug delivery and biomedical applications.


1. Gutierrez, D. D., Surtchev, E., Eiser, E. & Elsevier, C. J. Ru(II)-based metallosurfactant inverted aggregates. *Nano Lett.* **6**, 145–147 (2006).
2. de la Rica, R., Fratila, R. M., Szarpak, F. A., Huskens, J. & Velders, A. H. Multivalent nanoparticle networks as ultrasensitive enzyme sensors. *Angew. Chem., Int. Ed.* **50**, 5704–5707 (2011).
3. Lohmeijer, B. G. G. & Schubert, U. S. Supramolecular engineering with macromolecules: An alter concept for block copolymers. *Angew. Chem., Int. Ed.* **41**, 3825–3829 (2002).
4. Song, J., Zhou, J.-J. & Duan, H.-W. Self-assembled plasmonic vesicles of SERS-encoded amphiphilic gold nanoparticles for cancer cell targeting and traceable intracellular drug delivery. *J. Am. Chem. Soc.* **134**, 13458–13469 (2012).
5. Zhou, H.-Y., Su, G.-X., Jiao, P.-F. & Yan, B. Accelerating the multifunctionalization of therapeutic nanoparticles by using a multicomponent reaction. *Chem. Eur. J.* **18**, 5501–5505 (2012).
6. Connor, E. E., Mwamuka, J., Gole, A., Murphy, C. J. & Wyatt, M. D. Gold nanoparticles are taken up by human cells but do not cause acute cytotoxicity. *Small.* **1**, 325–327 (2005).
7. Nune, S. K. *et al.* Green nanotechnology from tea: phytochemicals in tea as building blocks for production of biocompatible gold nanoparticles. *J. Mater. Chem.* **19**, 2912–2920 (2009).
8. Daniel, M.-C. & Astruc, D. Gold nanoparticles: Assembly, supramolecular chemistry, quantum-size-related properties, and applications toward biology, catalysis, and nanotechnology. *Chem. Rev.* **104**, 293–346 (2004).
9. Giljohann, D. A. *et al.* Gold nanoparticles for biology and medicine. *Angew. Chem. Int. Ed.* **49**, 3280–3295 (2010).
10. Love, J. C., Estroff, J. A., Kriebel, J. K., Nuzzo, R. G. & Whitesides, G. M. Self-assembled monolayers of thiolates on metals as a form of nanotechnology. *Chem. Rev.* **105**, 1103–1169 (2005).
11. Ghosh, P. S., Kim, C. K., Han, G., Forbes, N. S. & Rotello, V. M. Efficient gene delivery vectors by tuning the surface charge density of amino acid-functionalized gold nanoparticles. *ACS Nano.* **2**, 2213–2218 (2008).
12. Steiniger, S. C. J. *et al.* Chemotherapy of glioblastoma in rats using doxorubicin-loaded nanoparticles. *Int. J. Cancer.* **109**, 759–767 (2004).
13. Aryal, S., Grailer, J. J., Pilla, S., Steeber, D. A. & Gong, S. Doxorubicin conjugated gold nanoparticles as water-soluble and pH-responsive anticancer drug nanocarriers. *J. Mater. Chem.* **19**, 7879–7884 (2009).
14. Panchagnula, R. Pharmaceutical aspects of paclitaxel. *Int. J. Pharm.* **172**, 1–15 (1998).
15. Han, S. Y. *et al.* Mineralized hyaluronic acid nanoparticles as a robust drug carrier. *J. Mater. Chem.* **21**, 7996–8001 (2011).
16. Lee, M. *et al.* Target-specific gene silencing of layer-by-layer assembled gold-cysteamine/siRNA/PEI/HA nanocomplex. *ACS Nano.* **5**, 6138–6147 (2011).
17. Kong, J. H., Oh, E. J., Chae, S. Y., Lee, K. C. & Hahn, S. K. Long acting hyaluronate-exendin 4 conjugate for the treatment of type 2 diabetes. *Biomaterials.* **31**, 4221–4128 (2010).
18. Annabi, B., Thibeault, S., Moumdjian, R. & Béliveau, R. Hyaluronan cell surface binding is induced by type I collagen and regulated by caveolae in glioma cells. *J. Biol. Chem.* **279**, 21888–21896 (2004).
19. Manju, S. & Sreenivasan, K. J. Gold nanoparticles generated and stabilized by water soluble curcumin-polymer conjugate: Blood compatibility evaluation and targeted drug delivery onto cancer cells. *Colloid Interface Sci.* **368**, 144–151 (2012).
20. Lee, H., Lee, K., Kim, I. K. & Park, T. G. Synthesis, characterization, and in *vivo* diagnostic applications of hyaluronic acid immobilized gold nanoprobes. *Biomaterials.* **29**, 4709–4718 (2008).
21. Zhang, X.-Q. *et al.* Strategy for increasing drug solubility and efficacy through covalent attachment to polyvalent DNA-nanoparticle conjugates. *ACS Nano.* **9**, 6962–6970 (2011).
22. Heo, D. N. *et al.* Gold nanoparticles surface-functionalized with paclitaxel drug and biotin receptor as theranostic agents for cancer therapy. *Biomaterials.* **33**, 856–866 (2012).
23. Chen, T. *et al.* Core-shell nanocarriers with ZnO quantum dots-conjugated Au nanoparticle for tumor-targeted drug delivery. *Carbohydr. Polym.* **92**, 1124–1132 (2013).
24. Eftink, M. R., Andy, M. L., Bystrom, K., Perlmutter, H. D. & Kristol, D. S. Cyclodextrin inclusion complexes: studies of the variation in the size of alicyclic guests. *J. Am. Chem. Soc.* **111**, 6765–6772 (1989).
25. Bakkour, Y. *et al.* Formation of cyclodextrin inclusion complexes with doxycyclin-hyclate: NMR investigation of their characterization and stability. *J. Inclusion Phenom. Macrocyclic Chem.* **54**, 109–114 (2006).
26. Alcaro, S. *et al.* Preparation, characterization, molecular modeling and in vitro activity of paclitaxel-cyclodextrin complexes. *Bioorg. Med. Chem. Lett.* **12**, 1637–1641 (2002).
27. Kang, J. *et al.* Cyclodextrin complexation: influence on the solubility, stability, and cytotoxicity of camptothecin, an antineoplastic agent. *Eur. J. Pharm. Sci.* **15**, 163–170 (2002).
28. Alvarez, M. M. *et al.* Optical absorption spectra of nanocrystal gold molecules. *J. Phys. Chem. B* **101**, 3706–3712 (1997).
29. Varnavski, O., Ramakrishna, G., Kim, J., Lee, D. & Goodson, T. Critical size for the observation of quantum confinement in optically excited gold clusters. *J. Am. Chem. Soc.* **132**, 16–17 (2010).
30. Panigrahi, S. *et al.* Synthesis and size-selective catalysis by supported gold nanoparticles: Study on heterogeneous and homogeneous catalytic process. *J. Phys. Chem. C* **111**, 4596–4605 (2007).
31. Citrin, P. H. & Wertheim, G. K. Photoemission from surface-atom core levels, surface densities of states, and metal-atom clusters: A unified picture. *Phys. Rev. B* **27**, 3176–3200 (1983).
32. Wang, H., Chen, Y., Li, X.-Y. & Liu, Y. Synthesis of oligo(ethylenediamino)-*β*-cyclodextrin modified gold nanoparticle as a DNA concentrator. *Mol. Pharm.* **4**, 189–198 (2007).
33. Elbakry, A. *et al.* Layer-by-layer assembled gold nanoparticles for siRNA delivery. *Nano Lett.* **9**, 2059–2064 (2009).

34. Schneider, G. & Decher, G. Functional core/shell nanoparticles via layer-by-layer assembly. Investigation of the experimental parameters for controlling particle aggregation and for enhancing dispersion stability. *Langmuir.* **24**, 1778–1789 (2008).
35. Griffin, J. *et al.* Size- and distance-dependent nanoparticle surface-energy transfer (NSET) method for selective sensing of hepatitis C virus RNA. *Chem. Eur. J.* **15**, 342–351 (2009).
36. Darbha, G. K., Ray, A. & Ray, P. C. Gold nanoparticle-based miniaturized nanomaterial surface energy transfer probe for rapid and ultrasensitive detection of mercury in soil, water, and fish. *ACS Nano.* **1**, 208–214 (2007).
37. Wang, F. *et al.* Doxorubicin-tethered responsive gold nanoparticles facilitate intracellular drug delivery for overcoming multidrug resistance in cancer cells. *ACS Nano.* **5**, 3679–3692 (2011).
38. Goodman, C. M., McCusker, C. D., Yilmaz, T. & Rotello, V. M. Toxicity of gold nanoparticles functionalized with cationic and anionic side chains. *Bioconjugte Chem.* **15**, 897–900 (2004).
39. Rosenholm, J. M., Peuhu, E., Eriksson, J. E., Sahlgren, C. & Linden, M. Targeted intracellular delivery of hydrophobic agents using mesoporous hybrid silica nanoparticles as carrier systems. *Nano Lett.* **9**, 3308–3311 (2009).
40. Lee, H., Mok, H., Lee, S., Oh, Y. K. & Park, T. G. Target-specific intracellular delivery of siRNA using degradable hyaluronic acid nanogels. *J. Control. Release.* **119**, 245–252 (2007).
41. Lee, H., Lee, K. & Park, T. G. Hyaluronic acid-paclitaxel conjugate micelles: Synthesis, characterization, and antitumor activity. *Bioconjugate Chem.* **19**, 1319–1325 (2008).
42. Luo, Y., Bernshaw, N. J., Lu, Z., Kopecek, J. & Prestwich, G. D. Targeted delivery of doxorubicin by HPMA copolymer-hyaluronan bioconjugates. *Pharm. Res.* **19**, 396–402 (2002).
43. Zhang, Z.-P., Lee, S. H. & Feng, S.-S. Folate-decorated poly(lactide-co-glycolide)-vitamin E TPGS nanoparticles for targeted drug delivery. *Biomaterials.* **28**, 1889–1899 (2007).

## Acknowledgments

We thank the 973 Program (2011CB932502), NNSFC (91227107 and 21272125) and the Program for New Century Excellent Talents in University (NCET-10-0500) for financial support.

## Author contributions

L.N., Y.Y. and S.Y. performed the synthesis and analyses of the AuNPs, HACD and HACD-AuNPs. C.Y. and Z.Y.M. performed the functional analyses of the drug@HACD-AuNPs. C.J.T. performed the cytotoxicity experiments. All authors discussed the results. L.N. and C.Y. wrote the main manuscript. L.N. prepared figures 1–6. L.Y. supervised the work and edited the manuscript. All authors reviewed the manuscript.

## Additional information

**Supplementary information** accompanies this paper at http://www.nature.com/scientificreports

**Competing financial interests:** The authors declare no competing financial interests.

**How to cite this article:** Li, N. *et al.* Polysaccharide-Gold Nanocluster Supramolecular Conjugates as a Versatile Platform for the Targeted Delivery of Anticancer Drugs. *Sci. Rep.* **4**, 4164; DOI:10.1038/srep04164 (2014).